Journal of Solid State Chemistry 184 (2011) 2374–2380

Contents lists available at ScienceDirect

Journal of Solid State Chemistry

journal homepage: www.elsevier.com/locate/jssc

Structural and magnetic study of $RFe_{0.5}V_{0.5}O_3$ (R=Y, Eu, Nd, La) perovskite compounds

M. Gateshki [a,1], L. Suescun [b,*], S. Kolesnik [c], J. Mais [c], B. Dabrowski [c,d]

[a] Bragg Institute, Australian Nuclear Science and Technology Organization, Menai, NSW 2234, Australia
[b] Cryssmat-Lab/Detema, Facultad de Química, Universidad de la República, P.O. Box 1157, Montevideo, Uruguay
[c] Physics Department, Northern Illinois University, DeKalb, IL 60115, USA
[d] Materials Science Division, Argonne National Laboratory, Argonne, IL 60439, USA

ARTICLE INFO

Article history:
Received 5 April 2011
Received in revised form
20 June 2011
Accepted 21 June 2011
Available online 29 June 2011

Keywords:
Perovskite
Magnetic structure
Rietveld analysis
Neutron powder diffraction
Antiferromagnetic
Cation ordering

ABSTRACT

B-site disordered $RFe_{0.5}V_{0.5}O_3$ compounds, with R=La, Nd, Eu and Y, have been prepared by solid-state reaction technique and their structures and magnetic properties have been investigated through X-ray powder diffraction, time-of-flight neutron powder diffraction and magnetization measurements at temperatures ranging from 5 to 700 K. The four compounds can be described as distorted perovskites with space group symmetry *Pbnm* and $a^+b^-b^-$ tilt system. The studied compounds also show antiferromagnetic ordering with Neel temperatures of 299, 304, 304, and 335 K respectively. The magnetic structures of R=La, Nd and Y compounds were determined from the neutron powder diffraction as G_z with observed magnetic moments of 2.55, 2.54 and 2.69μ_B at 30, 40 and 40 K, respectively.

1. Introduction

Materials from the families $RFeO_3$ and RVO_3, where R is a rare earth element or Y, have been extensively studied in the past due to their interesting magnetic and structural properties. These materials crystallize with orthorhombic perovskite structures (space group *Pbnm*, No. 62) with lattice constants $a \sim b \sim c/\sqrt{2}$, where the R-atoms occupy the twelve-coordinated A-sites of the perovskite structure and Fe/V atoms are located in the B-sites (centers of BO_6 octahedra). The octahedra formed by the oxygen atoms are slightly rotated (tilted) around the axes of the perovskite structure, which causes the orthorhombic distortion of the unit cell. At high temperatures the magnetic properties of $RFeO_3$ materials are determined by the indirect exchange Fe–O–Fe interactions, which lead to antiferromagnetic ordering with the Néel temperature T_N in the range between 620 K for $YFeO_3$ and 750 K for $LaFeO_3$ [1,2]. The orientation of the magnetic moments is of the G_x-type (magnetic moments parallel to the x-axis) and is not completely antiferromagnetic because the moments are slightly canted leading to the formation of a small net ferromagnetic component [1,3]. For $LaFeO_3$, it was found that the magnetic moments are directed along x with small components along y and z as well [4]. As the temperature is lowered to about 100–200 K, the competition of the Fe–Fe and R–Fe interactions leads to the so called spin–reorientation transition of the magnetic moments where they change direction from parallel to x to almost parallel to z (G_z-type antiferromagnetic). This effect has been observed for R=Nd, but not for R=Y, Eu, La. Some of the rare-earth orthoferrites (including $NdFeO_3$) have shown a long-range C-type antiferromagnetic ordering of the magnetic moments of R-atoms below temperatures of the order of 2–6 K [1,3]. The compounds of the RVO_3 family, which are typical Mott insulators, also show intricate magnetic and structural characteristics involving correlations between octahedral tilting, lattice distortions and orbital and spin ordering. For example, YVO_3 undergoes three phase transitions: a structural phase transition from orthorhombic (*Pbnm*) to monoclinic phase ($P2_1/a$) occurring concomitantly with G-type orbital ordering at 200 K, a magnetic transition to form a C-type antiferromagnetic arrangement of spins at 115 K and a transition to G-type spin and C-type orbital ordered state at 71 K [5–7]. On the other hand, $LaVO_3$ undergoes a transition to a G-type spin-ordered phase at around 140 K and a structural transition only a few degrees below this temperature [5]. In earlier studies it was reported that the two transitions occur simultaneously [8]. Given this variety of effects, it could be expected that including both Fe and V atoms in the same material would give rise to new and interesting properties such as

* Corresponding author.
E-mail address: leopoldo@fq.edu.uy (L. Suescun).
[1] Present address: PANalytical B.V., P.O. Box 13, 7600 AA Almelo, The Netherlands.

0022-4596/$ - see front matter © 2011 Elsevier Inc. All rights reserved.
doi:10.1016/j.jssc.2011.06.025

half-metallicity and magnetoresistance especially if ordered arrangement of the cations is formed. The only compounds where this idea was explored were $SrLaFeVO_6$ and $CaLaFeVO_6$ [9]. From powder X-ray diffraction measurements it was established that they have cubic perovskite structures with low degrees of cation ordering: 65% for $SrLaFeVO_6$ and 69% for $CaLaFeVO_6$ (50% corresponds to a completely disordered material and 100% to a completely ordered). In the same work by means of redox titration it was found that the oxidation state of V is 4. Both materials were found to be semiconducting and ferrimagnetically ordered with $T_C \sim 350$ K for the Sr compound and 200 K for the Ca-containing one.

In the present work we report the synthesis of the new $R Fe_{0.5}V_{0.5}O_3$ (R=Y, Eu, Nd, La) perovskite compounds and their characterization by means of X-ray and neutron powder diffraction and magnetic susceptibility measurements in a wide temperature range.

2. Experimental

2.1. Synthesis

The samples of $R Fe_{0.5}V_{0.5}O_3$ (R=Y, Eu, Nd, La) were prepared by solid-state reaction of pre-fired Y_2O_3, Eu_2O_3, Nd_2O_3, La_2O_3, Fe_2O_3 and V_2O_3. The starting stoichiometric mixture of thoroughly ground oxides was pressed in a 13 mm pellet under 5 ton and first fired in Ar at 1173 K for 12 h. The materials were then re-ground, pelletized and fired in pure Ar (> 99.999) at 1623 K for several 12 h periods with intermediate re-grindings. X-ray diffraction (XRD) data were collected after each firing using a Rigaku D-Max Powder Diffractometer with Cu$K\alpha$ radiation to check the phase composition of the samples. Even after the last treatment at the highest temperature all compounds except $LaFe_{0.5}V_{0.5}O_3$ showed the presence of small amounts of RVO_4 in the X-ray diffraction patterns that were not possible to completely eliminate by changing the synthesis conditions to gas mixtures of 0.33–1.00% H_2/Ar. The approximate amounts of impurity were 2.1(5) wt% for R=Y; 2.5(5) wt% for R=Eu and less than 1 wt% for R=Nd as extracted from Rietveld analysis of the XRD data.

2.2. Magnetic properties

Magnetization was measured by use of a Magnetic Property Measurement System (Quantum Design). Fig. 1 shows the temperature dependence of magnetization M for $R Fe_{0.5}V_{0.5}O_3$, measured on cooling in a magnetic field of 1 kOe. All the measured materials demonstrate antiferromagnetic transitions (T_N, determined from the maximum of the absolute value of the derivative dM/dT) at temperatures 299, 304, 304 and 335 K for R=La, Nd, Eu and Y, respectively. These transition temperatures close to room temperature lie between those for RVO_3 and $RFeO_3$, indicating mixed superexchange Fe–V interactions. The observed trend of T_N to increase with decrease in ionic radius of R^{3+} (from La to Y) is similar to the one observed for the G-type orbital ordering transition temperatures in RVO_3 [5].

Different and complex behavior of magnetization for $R Fe_{0.5}V_{0.5}O_3$ can be observed for different R at and below the magnetic transitions as observed for RVO_3 compounds [5,10]. A full description of this behavior is outside the scope of this work and will be published elsewhere.

2.3. Neutron and X-ray diffraction experiments and data analysis

Temperature-dependent time-of-flight (TOF) neutron powder diffraction (NPD) data were collected at the Special Environment

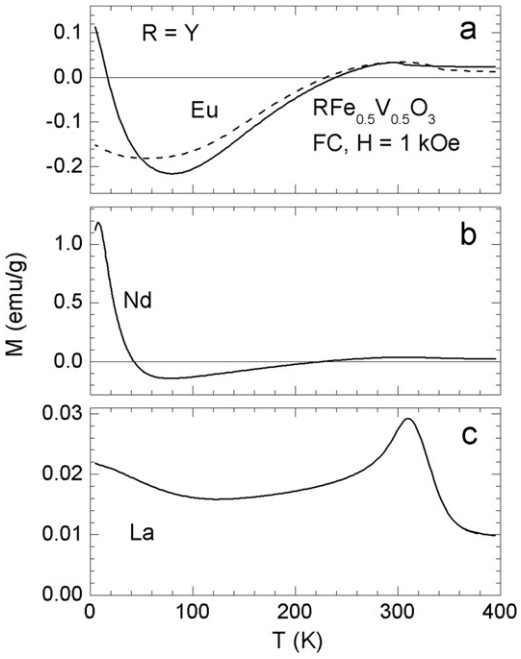

Fig. 1. Temperature dependence of magnetization for $R Fe_{0.5}V_{0.5}O_3$. The data were recorded on "field cooling" (FC) in a magnetic field of 1 kOe. Dashed line in top panel corresponds to $EuFe_{0.5}V_{0.5}O_3$.

Powder Diffractometer (SEPD) at Argonne's Intense Pulsed Neutron Source [11]. This instrument was equipped with four detector banks located at 2θ angles of 144°, 90°, 44° and 22°. The first three banks cover considerable Q-range and are suitable for structural refinement. The fourth one is used for detection of diffraction peaks in the low-Q-range. The samples consisting of ~5 g of the studied powders (with R=Y, Nd, La) were placed in a vanadium can with a diameter of 1 cm, sealed in He and inserted into a Hot-stage Displex cryofurnace used for controlling the temperature. Diffraction patterns were collected at different temperatures with 2 h of collection time for each temperature. Structural refinement and data correction were performed using the GSAS/EXPGUI suite of programs [12,13]. Oxygen stoichiometry was verified by refinement of oxygen site occupation factors converging to full occupancy within experimental error. Oxygen content was not refined in the last least-square cycle to avoid the addition of non-significant parameters to the final model. For all samples and temperatures, the structural models were refined simultaneously against the diffraction data from the first three detector banks (see Fig. 2). This reduces the effect of possible calibration problems and allows obtaining structural data with very high quality. The Eu-containing sample was not studied with neutron diffraction due to the high absorption cross section of ^{151}Eu isotope present in the natural isotopic distribution of Eu used for the sample preparation. Its room-temperature structure was refined from the collected X-ray data (Fig. 3) to compare it with isostructural compounds; thus, the structural parameters listed in Table 2 are not as precise for $R Fe_{0.5}V_{0.5}O_3$ as for other compounds.

3. Results and discussion

From the collected X-ray data it was established that, at room temperature, all of the studied materials have the orthorhombic perovskite structure typical of $GdFeO_3$. This structure has symmetry described by the space group *Pbnm* and presents octahedral tilting of the type $a^+b^-b^-$ [14], which involves in-phase

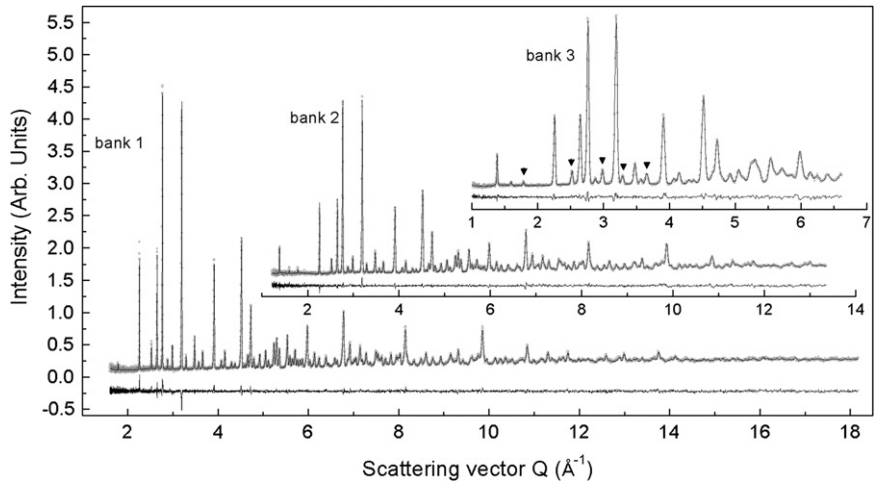

Fig. 2. Experimental diffraction profiles (symbols) of $LaFe_{0.5}V_{0.5}O_3$ collected at 300 K with the three detector banks (bank 1 at 144°; bank 2 at 90°; and bank 3 at 44°). The calculated and difference profiles (lines) are obtained after simultaneous Rietveld refinement of the crystal structure using the experimental profiles from the three banks. Triangles in the upper plot point to some of the diffraction peaks arising from in-phase octahedral rotations and La displacements.

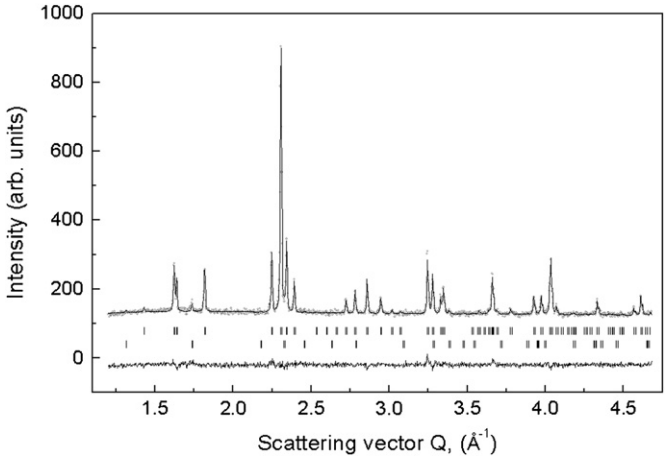

Fig. 3. Experimental (symbols), calculated and difference diffraction profiles (lines) for the Rietveld refinement of $EuFe_{0.5}V_{0.5}O_3$ at 300 K. The bars in the lower part of the graph represent the Bragg positions of $EuFe_{0.5}V_{0.5}O_3$ at 300 K (upper set of bars) and the impurity $EuVO_4$ (lower set).

rotations of the octahedra from two adjacent layers around one of the axes of the parent cubic perovskite structure and out-of-phase rotations with equal magnitudes around the other two axes. The observation of the orthorhombic structure in the studied materials is not an unexpected result as all of the RMO_3 compounds with R=Y, Nd, Eu, La and M=Fe,V crystallize with the same type of structure. Interesting is the case of $LaFe_{0.5}V_{0.5}O_3$ for which the splitting of the diffraction lines characteristic of orthorhombic distortion of the unit cell could not be observed in the X-ray data. This could be an indication of a cubic structure, however some low-intensity reflections incompatible with such cubic perovskite (space group *Pm3m*) structure were observed in the neutron data (marked with arrows in Fig. 2) showing that the actual symmetry is lower. On the other hand, an orthorhombic structure with a pseudo-cubic unit cell can account for these low-intensity reflections by allowing both octahedral rotations and *R*-cation displacements. In a similar way, early studies of both $LaFeO_3$ [15] and $LaVO_3$ [16] reported that these compounds have cubic perovskite structures while later more detailed studies [17,18] showed that these compounds have orthorhombic structures with pseudo-cubic unit cells.

The NPD data collected at different temperatures from the samples with R=Y, Nd, La (Fig. 4) show that the intensities of some of the diffraction peaks increase significantly at lower temperatures while others remain unchanged. This result is readily explained with the presence of G-type antiferromagnetic ordering (Fig. 5) in accordance with previous magnetic structures described in the $RFeO_3$ and RVO_3 systems [1,3,5] and the magnetic susceptibility measurements. No other temperature-dependent changes were observed in the diffraction patterns indicating that there are no structural transformations in the temperature interval covered here. The structural details and the values of the magnetic moments of all compounds were refined assuming orthorhombic structures with *Pbnm* symmetry and are given in Tables 1–3. As seen, in all structural models the *R* cations are displaced from the positions they occupy in the cubic perovskite structure (0,0,1/4) and the same is true for the two types of oxygen atoms O1 (1/2,0,1/4) and O2 (3/4,1/4,0). For $LaFe_{0.5}V_{0.5}O_3$, the diffraction peaks originating from the octahedral rotations and *R*-cation displacements are clearly visible (marked with triangles in Fig. 2), thus confirming that the structure of this compound is indeed orthorhombic and not cubic as suggested by the similar values of the lattice constants (see Fig. 6).

The variations of the lattice constants with the temperature and with the tolerance factor of the studied compounds are shown in Figs. 6 and 7, respectively. The tolerance factor $t = d_{A-O}/\sqrt{2}d_{B-O}$, which is a measure of the mismatch between the size of the A-site cation and the interstitial space between the BO_6 octahedra was calculated using the geometric average of all twelve A–O and six B–O distances. Value of t=1 is the ideal for stabilizing the cubic perovskite structure and corresponds to the case where the size of the A-cation matches perfectly the space between the octahedra. In Fig. 6, it can be observed that the lattice constants increase slightly with temperature due to thermal expansion. On the other hand, as the tolerance factor increases approaching 1, the orthorhombic distortion decreases and for $LaFe_{0.5}V_{0.5}O_3$ (t=0.981) the three lattice parameters become practically indistinguishable (Fig. 7). The inset of Fig. 7 shows the variation of the fractional coordinates of the A-cations as a function of the tolerance factor and again it can be observed that at values of t closer to 1 the structure becomes more pseudo-cubic as suggested by the decreased displacement of the A-cations from their positions in the cubic structure (x_A=0, y_A=0).

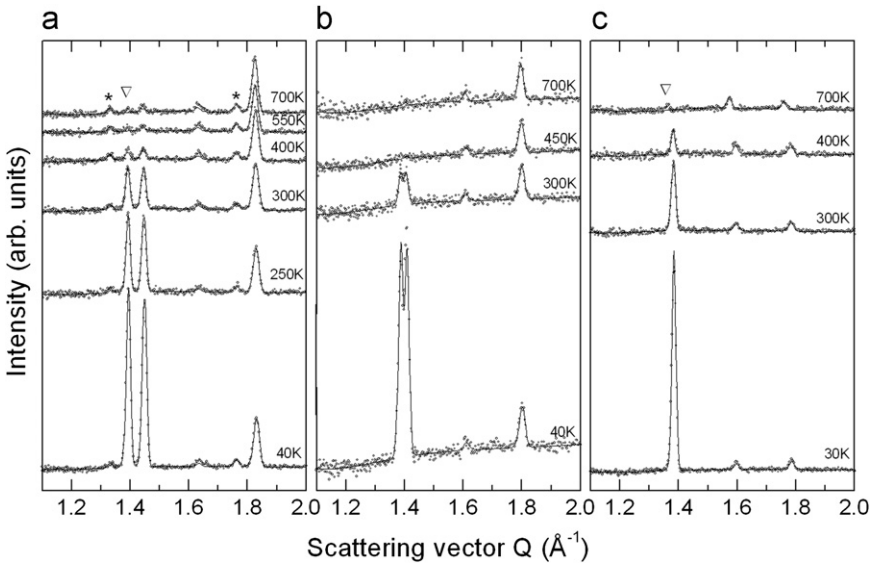

Fig. 4. Variation with temperature of the diffraction profiles of $YFe_{0.5}V_{0.5}O_3$ (a) $NdFe_{0.5}V_{0.5}O_3$ (b) and $LaFe_{0.5}V_{0.5}O_3$ (c). Peaks marked with asterisks are due to YVO_4. The strong increase of the peaks around 1.4 $Å^{-1}$ at low temperatures is due to the antiferromagnetic ordering of the magnetic moments of Fe and V atoms. The position of (011) reflection at 700 K is marked with a down triangle.

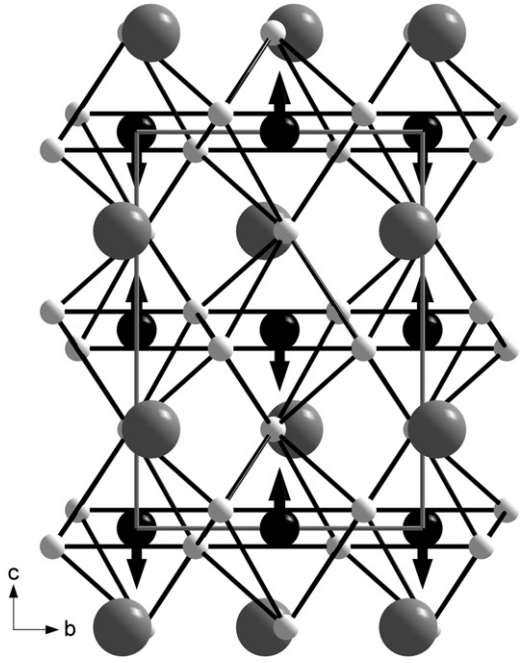

Fig. 5. Schematic representation of the orthorhombic perovskite structure of $RFe_{0.5}Ni_{0.5}O_3$ structure (R=A, Fe, Ni=B). The gray, black and white circles represent the A and B cations and O anions, respectively. The thin lines outline the unit cell and the thicker lines show the edges of BO_6 octahedra. The arrows give the directions of the magnetic moments on B atoms for G-type antiferromagnetic ordering observed in the studied compounds.

At this point we would like to make a comment on the B-site cation ordering (or lack thereof) in the studied samples. In many cases where the B-sites of the perovskite structure are occupied by two different types of cations these can order, usually in a rock-salt manner, so as to reduce the electrostatic energy. The presence and degree of ordering depends on many factors: sizes of the A-cations, ionization energies, synthesis temperature, etc., but the most important factor is the charge difference between the two types of B-cations. It is generally assumed [19] that if the charge difference Δq is >2 the compound will present at least partial ordering and if $\Delta q < 2$, the cations will remain disordered (randomly distributed). Preliminary Mossbauer spectroscopy experiments suggest that the oxidation state of Fe is 3+, therefore V^{3+} should also be present in the compounds, meaning that formation of ordered arrangement of the cations in the studied compounds is unlikely. The presence of rock-salt cation ordering in orthorhombic perovskites is usually established by the observation of reflections of the type *0kl* ($k,l=2n+1$) in the experimental diffraction patterns. For the materials studied here, these characteristic reflections were not observed in the X-ray measurements, however given the similar atomic numbers of Fe and V these atoms have comparable scattering power for the radiation used and it may be very difficult to observe the order-related reflections even if such order existed. In the case of NPD measurements the coherent scattering lengths of Fe and V are very different ($b_{Fe}=9.45$, $b_V=-0.443$ fm) [20] and in principle it should be possible to observe cation ordering. However, in the studied materials the reflections related to the cation ordering overlap with the magnetic ones, which results from the fact that in G-type antiferromagnetic ordering the magnetic moments form the same rock-salt pattern expected for the cation ordering. Thus, cation ordering can be observed only at temperatures above T_N. In the experimental diffraction patterns of $YFe_{0.5}V_{0.5}O_3$ at 550 and 700 K and those of $LaFe_{0.5}V_{0.5}O_3$ at 700 K (shown in Fig. 4a and c), very weak diffraction peaks can be observed in the position of (011) Bragg reflection. If these peaks are interpreted as an evidence of cation ordering the degree of such ordering will be extremely small $\sim$54%. Another plausible explanation for these weak peaks in $LaFe_{0.5}V_{0.5}O_3$ pattern at 700 K is the presence of small amounts of $LaFeO_3$ impurity, which is antiferromagnetic up to 740 K. For $YFe_{0.5}V_{0.5}O_3$ the possible presence of $YFeO_3$ would not explain the observation of the mentioned peaks due to the lower T_N (620 K) of this compound. Given that the materials were prepared from stoichiometric mixtures and the only impurities found were RVO_4, it is not unreasonable to expect the formation of $RFeO_3$; however the amount of this impurity in the samples would never exceed 5% in weight; therefore, it is highly improbable that magnetic peaks from it would account for the observed intensities. Only very high-resolution diffraction measurements or single crystal neutron diffraction could confirm this as the lattice constants of $RFeO_3$ are very similar to those of

Table 1
Structural details of $YFe_{0.5}V_{0.5}O_3$ obtained at different temperatures. The atoms occupy the following Wyckoff positions in *Pbnm*, Y (4*c*: *x*,*y*, 1/4), Fe/V (4*b*: 1/2,0,0), O1 (4*c*: *x*,*y*, 1/4) and O2 (8*d*: *x*,*y*, *z*).

Temp. (K)	40	250	300	400	550	700
a (Å)	5.27438(26)	5.2800(4)	5.28387(27)	5.28893(29)	5.29655(30)	5.29861(30)
b (Å)	5.59185(28)	5.5959(4)	5.59692(29)	5.59757(30)	5.60071(31)	5.60205(31)
c (Å)	7.5759(4)	7.5902(5)	7.5966(4)	7.6045(4)	7.6158(4)	7.6190(4)
Y						
x	0.01884(13)	0.01821(18)	0.01792(14)	0.01717(14)	0.01726(15)	0.01707(14)
y	0.06928(9)	0.06848(13)	0.06831(10)	0.06778(10)	0.06719(11)	0.06715(10)
U_{iso} (Å^2)	0.00181(15)	0.00396(23)	0.00523(18)	0.00644(19)	0.00800(21)	0.00842(20)
Fe/V						
U_{iso} (Å^2)	0.00216(22)	0.00362(27)	0.00455(21)	0.00546(22)	0.00644(24)	0.00690(23)
O1						
x	0.61133(15)	0.61059(21)	0.61068(16)	0.61018(16)	0.60997(17)	0.60976(16)
y	−0.03917(14)	−0.03949(20)	−0.03947(15)	−0.03948(15)	−0.03966(16)	−0.03963(15)
U_{eq} (Å^2)	0.00329	0.00499	0.00593	0.00705	0.00849	0.00894
O2						
x	0.80878(10)	0.80786(14)	0.80809(11)	0.80798(11)	0.80798(12)	0.80804(11)
y	0.19705(11)	0.19560(15)	0.19596(11)	0.19568(11)	0.19517(12)	0.19570(11)
z	−0.05694(7)	−0.05674(10)	−0.05652(7)	−0.05659(7)	−0.05642(8)	−0.05642(7)
U_{eq} (Å^2)	0.00401	0.00568	0.00676	0.00776	0.00960	0.00996
μ_B	2.699(15)	1.860(18)	1.323(13)	0.540(18)	–	–
R_{wp} (%) (all data)	4.84	6.38	4.71	4.52	3.06	4.34
χ^2	1.567	1.207	1.383	1.418	1.275	1.429

Table 2
Structural details of $EuFe_{0.5}V_{0.5}O_3$ at 300 K obtained from XRD data and of $NdFe_{0.5}V_{0.5}O_3$ obtained at different temperatures from NPD data. The atoms occupy the following Wyckoff positions in *Pbnm*, Eu/Nd (4*c*: *x*, *y*, 1/4), Fe/V (4*b*: 1/2,0,0), O1 (4*c*: *x*,*y*, 1/4) and O2 (8*d*: *x*,*y*, *z*).

	$EuF_{0.5}V_{0.5}O_3$	$NdF_{0.5}V_{0.5}O_3$			
Temp. (K)	293	40	300	450	700
a (Å)	5.36992(24)	5.44260(18)	5.44970(18)	5.45733(16)	5.46770(17)
b (Å)	5.59751(26)	5.56990(11)	5.56823(11)	5.57246(10)	5.57803(10)
c (Å)	7.6745(4)	7.7315(3)	7.7516(3)	7.76303(26)	7.77809(28)
Eu/Nd					
x	0.0158(11)	0.01180(19)	0.01001(23)	0.00983(20)	0.00922(24)
y	0.0579(4)	0.05028(12)	0.04797(15)	0.04731(12)	0.04578(16)
U_{iso} (Å^2)	0.0129(21)	0.00171(18)	0.00581(24)	0.00728(21)	0.00976(28)
Fe/V					
U_{iso} (Å^2)	0.0179(27)	0.00232(26)	0.0056(3)	0.00528(29)	0.0073(4)
O1					
x	0.581(4)	0.58688(24)	0.58658(27)	0.58630(23)	0.58634(29)
y	−0.017(3)	−0.02291(20)	−0.02266(23)	−0.02259(21)	−0.02297(25)
U_{eq} (Å^2)	0.013(7)	0.00478	0.00778	0.01004	0.01212
O2					
x	0.799(3)	0.79714(15)	0.79523(17)	0.79507(15)	0.79449(18)
y	0.197(3)	0.20615(14)	0.20582(16)	0.20569(14)	0.20611(17)
z	−0.0485(22)	−0.04601(11)	−0.04525(13)	−0.04507(11)	−0.04468(14)
U_{eq} (Å^2)	0.013(7)	0.00475	0.00802	0.00958	0.01198
μ_B	–	2.539(20)	0.56 (3)	–	–
R_{wp} (%) (all data)	3.09	4.66	4.85	4.01	4.70
χ^2	1.346	1.387	1.206	1.270	1.211

$RFe_{0.5}V_{0.5}O_3$. Further studies will be required to clarify whether the peaks observed in the NPD data are due to cation ordering or other effects.

The arrangement of magnetic moments below T_N in the three $LaFe_{0.5}V_{0.5}O_3$, $NdFe_{0.5}V_{0.5}O_3$ and $YFe_{0.5}V_{0.5}O_3$ compounds could be described as G_z implying that magnetic moments are oriented along *c*-axis but alternate in direction among neighboring Fe/V cations. The refinement of magnetic moments in the Shubnikov space group [21] *Pbn′m′* (transformation of *Pn′m′a* magnetic space group number 62.6.507 according to Litvin tables [22]) was performed using the color symmetry capabilities of GSAS. Refined magnetic moments for average Fe/V sites are shown in Tables 1–3. Since oxygen-mediated Fe–Fe and V–V magnetic interactions are expected to be antiferromagnetic according to Goodenough–Kanamori rules and the number of Fe–V interactions of ferromagnetic character are reduced due to the disorder on the B-site, the magnetic moment of Fe/V sites is slightly lower than the expected average contribution of both cations. Observed values at

Table 3
Structural details of $LaFe_{0.5}V_{0.5}O_3$ obtained at different temperatures. The atoms occupy the following Wyckoff positions in *Pbnm*, La (4*c*: *x*,*y*, 1/4), M (4*b*: 1/2,0,0), O1 (4*c*: *x*,*y*, 1/4) and O2 (8*d*: *x*,*y*, *z*).

Temp. (K)	30	300	400	700[a]
a (Å)	5.5519(3)	5.5597(7)	5.5660 (4)	5.5767(12)
b (Å)	5.5548(3)	5.5571(7)	5.5608(3)	5.5657(12)
c (Å)	7.8356(4)	7.8523(10)	7.8603(5)	7.8773(20)
La				
x	0.00600(27)	0.0055(4)	0.0047(4)	0.0051(13)
y	0.03256(12)	0.02952(19)	0.02802(16)	0.0251(6)
U_{iso} (Å^2)	0.00207(18)	0.0076(5)	0.00737(20)	0.0105(8)
Fe/V				
U_{iso} (Å^2)	0.300(22)	0.0082(6)	0.00601(26)	0.0078(10)
O1				
x	0.5758(3)	0.5758(5)	0.5739(4)	0.5789(12)
y	−0.01228(25)	−0.0123(4)	−0.0117(3)	−0.0142(11)
U_{iso} (Å^2)	0.00507(23)	0.0106(7)	0.0099(3)	0.0153(16)
O2				
x	0.78443(19)	0.7815(3)	0.78125(24)	0.7790(8)
y	0.21839(20)	0.2178(3)	0.21808(25)	0.2220(8)
z	−0.03917(13)	−0.03770(22)	−0.03801(17)	−0.0373(5)
U_{iso} (Å^2)	0.00508(17)	0.0116(7)	0.01013(24)	0.0143(11)
μ_B	2.497(21)	1.317(15)	0.665(18)	–
R_{wp} (%) (all data)	5.70	4.94	5.50	8.94
χ^2	1.429	1.346	1.330	6.183

[a] Data collected in Bank 1 at 700 K was excluded from the refinement due to the presence of multiple electronic errors in the counters included in this bank.

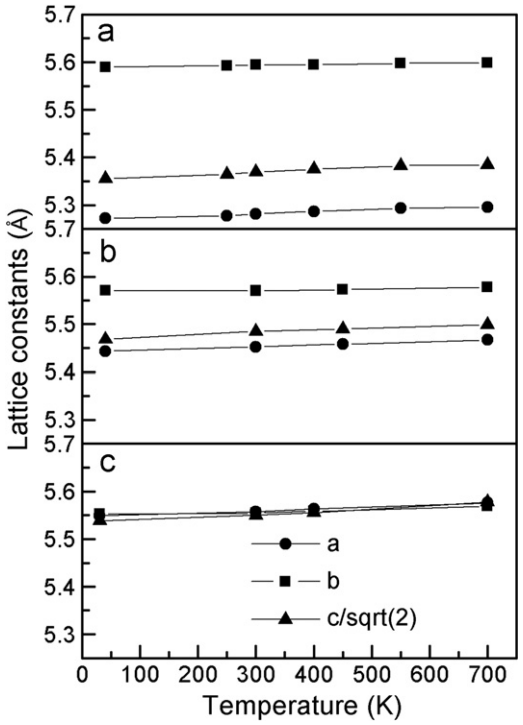

Fig. 6. Variation of lattice constants of $YFe_{0.5}V_{0.5}O_3$ (a), $NdFe_{0.5}V_{0.5}O_3$ (b) and $LaFe_{0.5}V_{0.5}O_3$ (c) with the temperature: (a) circles, (b) squares and (c) $c/\sqrt{2}$ triangles.

30 and 40 K are approximately $1\mu_B$ below to the expected $3.5\mu_B$ (at 0 K) for the average of high spin Fe^{3+} (d^5, $S=5/2$) and V^{3+} (d^2, $S=1$).

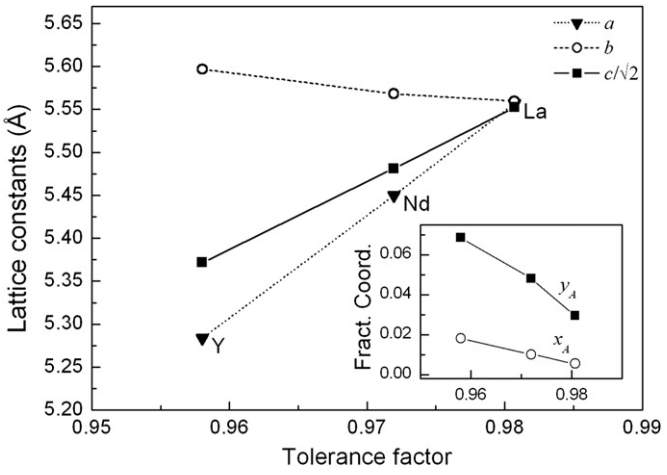

Fig. 7. Variation of the lattice constants and the *y* fractional coordinate (inset) of the A-cations at 300 K of the studied compounds as a function of their tolerance factor.

Further details of the crystal structure investigations may be obtained from Fachinformationszentrum Karlsruhe, 76344 Eggenstein-Leopoldshafen, Germany (fax: (+49)7247–808-666; e-mail:crysdata@fiz-karlsruhe.de, http://www.fiz-karlsruhe.de/ecid/Internet/en/DB/icsd/depot_anforderung.html) on quoting the deposition numbers CSD-422655 for $EuFe_{0.5}V_{0.5}O_3$, CSD-42265 (6–9) for $LaFe_{0.5}V_{0.5}O_3$, CSD-42266(1–4) for $NdFe_{0.5}V_{0.5}O_3$ and CSD-4226(65–70) for $YFe_{0.5}V_{0.5}O_3$.

4. Conclusions

Compounds in the $RFe_{0.5}V_{0.5}O_3$ system (R=La, Nd, Eu and Y) show orthorhombic *Pbnm* perovskite structure with a disordered arrangement of Fe^{3+} and V^{3+} cations in a tilted octahedra network. Unit cell parameters and tolerance factors evolve with rare-earth ionic radii towards a pseudo-cubic structure similar to that observed in other La perovskites. Although there seems to be no driving force for Fe/V ordering, evidence of it is observed by high-temperature neutron powder diffraction indicating a possible 54% site order (50% fully disordered; 100% fully ordered) that deserves further investigation. Antiferromagnetic ordering of spins is observed, with observed magnetic moments and Néel temperatures intermediate between RVO_3 and $RFeO_3$ compounds in zero field.

Acknowledgments

Work at NIU was supported by the NSF-DMR-0706610 (B.D., S.K., J.M.). Argonne National Laboratory's work was supported by the U.S. Department of Energy, Office of Science, Office of Basic Energy Sciences, under contract DE-AC02-06CH11357 (B.D.). L.S. is indebted to PEDECIBA, CSIC and ANII (Uruguayan organizations).

References

[1] R.L. White, J. Appl. Phys. 40 (1969) 1061–1069.
[2] W.C. Koehler, E.O. Wollan, M.K. Wilkinson, Phys. Rev. 118 (1960) 58–70.
[3] W. Slawinski, R. Przenioslo, I. Sosnowska, E. Suard, J. Phys.: Condens. Matter 17 (2005) 4605–4614.
[4] T. Peterlin-Neumaier, E. Steichele, J. Magn. Magn. Mater. 59 (3–4) (1986) 351–356.
[5] S. Miyasaka, Y. Okimoto, M. Iwama, Y. Tokura, Phys. Rev. B: Condens. Matter Mater. Phys 68 (10) (2003) 100406(R).
[6] J.B. Goodenough, J.-S. Zhou, J. Mater. Chem. 17 (23) (2007) 2394–2405.
[7] G.R. Blake, T.T.M. Palstra, Y. Ren, A.A. Nugroho, A.A. Menovsky, Phys. Rev. B: Condens. Matter Mater. Phys 65 (17) (2002) 174112.
[8] P. Bordet, C. Chaillout, M. Marezio, Q. Huang, A. Santoro, S.-W. Cheong, H. Takagi, C.S. Oglesby, B. Batlogg, J. Solid State Chem. 106 (2) (1993) 253–270.

[9] K. Ramesha, J. Gopalakrishnan, V. Smolyaninova, R.L. Greene, J. Solid State Chem. 162 (2) (2001) 250–253.
[10] H.C. Nguyen, J.B. Goodenough, Phys. Rev. B: Condens. Matter Mater. Phys. 52 (1) (1995) 324–334.
[11] J.D. Jorgensen, J. Faber Jr., J.M. Carpenter, R.K. Crawford, J.R. Haumann, R.L. Hitterman, R. Kleb, G.E. Ostrowski, F.J. Rotella, T.G. Worlton, J. Appl. Cryst. 22 (1989) 321–333.
[12] A.C. Larson, R.B. Von Dreele, General Structure Analysis System (GSAS), Los Alamos National Laboratory Report LAUR 86-748, 2004.
[13] B.H. Toby, J. Appl. Cryst. 34 (2001) 210–213.
[14] A.M. Glazer, Acta Crystallogr. Sect. B: Struct. Sci. 28 (1972) 3384–3392.
[15] W.C. Koehler, E.O. Wollan, J. Phys. Chem. Solids 2 (2) (1957) 100–106.
[16] A. Wold, R. Ward, J. Amer. Chem. Soc. 76 (4) (1954) 1029–1030.
[17] H. Taguchi, Y. Masunaga, K. Hirota, O. Yamaguchi, Mater. Res. Bull. 40 (5) (2005) 773–780.
[18] H. Seim, H. Fjellvag, B.C. Hauback, Acta Chem. Scand. 52 (9) (1998) 1301–1306.
[19] M.T. Anderson, K.B. Greenwood, G.A. Taylor, K.R. Poeppelmeier, Prog. Solid State Chem. 22 (1993) 197–233.
[20] A.-J. Dianoux, G. Lander (Eds.), Neutron Data Booklet, OCP Science, 2003.
[21] A.V. Shubnikov, N.V. Belov, Colored Symmetry, Pergamon, Oxford, 1964.
[22] D. Litvin, Acta Crystallogr. A64 (2008) 419–424.